Vietnam Journal of Earth Sciences, 43(3), 285-300, https://doi.org/10.15625/2615-9783/16196

Vietnam Academy of Science and Technology
Vietnam Journal of Earth Sciences
http://www.vjs.ac.vn/index.php/jse

30-year changes of natural forests under human activities in the Indochina peninsula - case studies in Cambodia, Laos and Vietnam

Nguyen Dinh Duong*, Lai Vinh Cam

Institute of Geography, Vietnam Academy of Science and Technology, Hanoi, Vietnam

Received 06 February 2021; Received in revised form 20 May 2021; Accepted 18 June 2021

ABSTRACT

Natural forests are a basic component of the earth's ecology. It is essential for biodiversity, hydrological cycle regulation, and environmental protection. Natural forests are gradually degraded and reduced due to timber logging, conversion to cropland, production forests, commodity trees, and infrastructure development. Decreasing natural forests results in loss of valuable habitats, land degradation, soil erosion, and imbalance of water cycle on the regional scale. Thus, operational monitoring of natural forest cover change has been in the interest of scientists for a long time. Current forest mapping methods using remotely sensed data provide limited capability to separate natural forests and planted forests. Natural forest statistics are often generated using official forestry national reports that have different bias levels due to different methodologies applied in different countries in forest inventory. Over the last couple of decades, natural forests have been over-exploited for various reasons. This led to forest cover degradation and water regulation capability, which results in extreme floods and drought of a watershed in general. This situation demands an urgent need to develop a fast, reliable, and automated method for mapping natural forests. In this study, by applying a new method for mapping natural forests by Landsat time series, the authors succeeded in mapping changes of natural forests of Cambodia, Laos, and Vietnam from 1989 to 2018. As a focused study area, three provinces: Ratanakiri of Cambodia, Attapeu of Laos, and Kon Tum of Vietnam were selected. The study reveals that after 30 years, 51.3% of natural forests in Ratanakiri, 27.8% of natural forests in Attapeu, and 50% of natural forests in Kon Tum were lost. Classification results were validated using high spatial resolution imagery of Google Earth. The overall accuracy of 99.3% for the year 2018 was achieved.

Keywords: Natural forest, Landsat, time series, simplified spectral patterns, automated classification, human activity, phenology.

1. Introduction

Natural forest is essential for biodiversity and environmental protection and socio-economy and the living conditions of forest-dependent populations (Stibig et al., 2007). Natural forests are gradually degraded and reduced due to timber logging, conversion to cropland, production forest, commodity trees, and infrastructure development. Decreasing natural forests results in loss of valuable habitats, land degradation, soil erosion, and

*Corresponding author, Email: ndduong@ig.vast.vn

imbalance of water cycle on a regional scale (Dennis et al., 2008). Thus, operational monitoring of natural forest cover change has been in the interest of scientists for a long time.

Indochina Peninsula or mainland Southeast Asia is the continental portion of Southeast Asia that includes Cambodia, Laos, Myanmar, Peninsular Malaysia, Thailand, and Vietnam. The forests of Southeast Asia are species-rich and provide essential ecological and economic functions (FAO, 2005), and comprises about 15% of the World's tropical forests (FAO, 1995). However, they also exhibit high rates of deforestation and degradation (Hughes, A.C., 2017). According to the FAO's report on the state of the World's forests (FAO, 2005), between 2000 and 2005, the rate of annual change of forests in Vietnam was +2%, in Lao P.D.R. -0.5% and in Cambodia -2%. The trends of forest changes were thoroughly reverse, and it is interesting to find out the drivers of those changes.

Current forest mapping methods using remotely sensed data provide limited capability to separate natural and planted forests. To separate natural forests from planted forests, we need to use time-series data and phenology of vegetation cover.

Methods for monitoring forest cover using Landsat time series (LTS) have been extensively studied during the last two decades. In general, the application of LTS for forest mapping can be categorized into two types: image classification and trajectory-based analysis (Banskota et al., 2014). In image classification-based analysis, individual images are separately classified, thereby minimizing radiometric calibration problems between dates (Coppin and Bauer, 1996). Trajectory-based approaches utilize the temporal patterns of spectral variables to detect disturbance types and magnitude. Unlike classification, it involves the analysis of a time series of single spectral variables. It can be further divided into 4 categories: (i) threshold-based change detection, (ii) single curve fitting, (iii) hypothesized curve fitting, and (iv) trajectory segmentation (Banskota et al., 2014).

Analysis of LTS requires careful image selection and pre-processing. Images of LTS are selected according to image quality and acquisition dates. The rules for selecting the best available pixel observation can be related to nearness to a target day of year and avoidance of atmospheric interference (be it cloud, haze, or resultant shadows) or prioritizing a particular sensor (White et al., 2014).

Radiometric correction and atmospheric correction also play important roles in the development of LTS. Radiometric correction includes calibration to radiance or at-satellite reflectance, while the atmospheric correction is performed to achieve minimal radiometric differences between images observed at a different time.

In this study, by application of automated classification method of land cover using the simplified spectral patterns with Landsat time series from 1989 to 2018 (Duong, 2020), the authors examined changes of forest cover of provinces Ratanakiri of Cambodia, Attapeu of Laos, and Kon Tum of Vietnam. The natural forest was assumed as a forest, which is not disturbed for 30 years. More than 2000 Landsat scenes of sensors TM, ETM+ and OLI were used for the research. The automated classification was conducted with basic land cover categories: Cloud, cloud shadow, water, wetland, closed forest, open forest, and bare land. Forest area that was changed to bare land is classified later as an area of intense human activities. The study showed that the proposed method for mapping natural forests is stable, independent, and uniform for natural forest inventory in large areas. The advantage of the newly proposed method is that it provides statistical data and spatiotemporal patterns on how the natural forest was reduced across time.

As a focused study area, three provinces: Ratanakiri of Cambodia, Attapeu of Laos, and Kon Tum of Vietnam were selected. The study reveals that after 30 years, 51.3% of natural forests in Ratanakiri, 27.8% of natural forests in Attapeu, and 50% of natural forests in Kon Tum were lost. Classification results were validated using high spatial resolution imagery of Google Earth. The overall accuracy of 99.3% for the year 2018 was achieved.

2. Materials and Methods

2.1. Study area

As representative study areas for Cambodia, Laos, and Vietnam, we selected three neighboring provinces: Ratanakiri of Cambodia, Attapeu of Laos, and Kon Tum of Vietnam. These provinces situate in the western side of the Truong Son range, so they are of similar climate characteristics (Fig. 1). In the study area, there are two distinct seasons: dry and rainy. The rainy season starts in May and ends in October. The dry season lasts from November to April annually. Due to the influences of the monsoon climate, there is a low opportunity to obtain a cloud-free image, especially during the rainy season. The prevalent vegetation cover of the study area is evergreen. However, there are also deciduous broad-leaved forests that lose their leaves during the dry season.

Figure 1. Study area with three provinces of Cambodia, Laos, and Vietnam. Ratanakiri is colored in violet, Attapeu in red and Kon Tum in blue

2.2. Landsat time series

2.2.1. Landsat collection 1 Level 1

LTS is composed of Landsat Collection 1 Level-1 data. Precision (ground control) and terrain corrected products are labeled with the L1TP designation. Terrain and systematically corrected products are labeled as L1GT. Systematically corrected products are labeled as L1 GS. OLI/TIRS products are either L1TP or L1GT, and ETM+, TM, and MSS products are L1TP, L1GT, or L1 GS. Radiometric and geometric data quality characteristics are available in sensor-, scene-, and pixel-level metadata (USGS, 2019a). The Landsat Collection 1 Level-1 is available on the website https://earthexplorer.usgs.gov/ for downloading.

2.2.2. Image selection

Forest types in the study area are of two: evergreen and deciduous broadleaf. Around the year, while the deciduous broadleaf forest loses leaves during the dry season, the evergreen forest has stable leaf coverage. Forest with no leaves often causes to miss classification, and therefore we selected images besides the dry season for the research. Images of months from May to December for the period from 1989 to 2018 were downloaded from the website https://earthexplorer.usgs.gov/. Five scenes cover the study area with path/row numbers 124/49, 124/50, 124/51, 125/50, and 125/51. The total number of images used for the research was about 2000.

2.2.3. Computation of Top of Atmosphere Reflectance

Before analysis, digital numbers (DN) of pixels were converted to top of atmosphere (TOA) reflectance to minimize image-to-image variability. There are three advantages of using TOA reflectance instead of at-sensor spectral radiance. First, it removes the cosine effect of different solar zenith angles due to the time difference between data acquisitions. Second, TOA reflectance compensates for different values of the exoatmospheric solar irradiance arising from spectral band differences. Third, the TOA reflectance corrects for the variation in the Earth-Sun distance between different data acquisition dates. These variations can be significant geographically and temporally. The TOA reflectance of the Earth is computed according to the equation (1):

$$\rho_\lambda = \frac{\pi . L_\lambda . d^2}{ESUN_\lambda . \cos\theta_s} \quad (1)$$

Where

ρ_λ = Planetary TOA reflectance [unit less]

π Mathematical constant equal to ~3.14159 [unit less]

L_λ = Spectral radiance at the sensor's aperture [W/(m^2 sr μm)]

d = Earth-Sun distance [astronomical units]

$ESUN_\lambda$ = Mean exoatmospheric solar irradiance [W/(m^2 μm)]

θ_s = Solar zenith angle [degrees]

Conversion of DN to TOA reflectance was carried out differently for sensors TM, ETM+ and OLI.

For OLI sensor, conversion of Level 1 DN to TOA reflectance is done by equation (2) (USGS, 2015).

$$\rho'_\lambda = M_\rho . Q_{cal} + A_\rho \quad (2)$$

Where

ρ'_λ = TOA Planetary Spectral Reflectance, without correction for solar angle (unitless).

M_ρ = Reflectance multiplicative scaling factor for the band. (REFLECTANCEW_MULT_BAND_n from the metadata).

A_ρ = Reflectance additive scaling factor for the band (REFLECTANCE_ADD_BAND_N from the metadata).

Q_{cal} = Level 1 pixel value in DN

The ρ'_λ is not true TOA Reflectance, because it does not contain a correction for the solar elevation angle. This correction factor is left out of the Level 1 scaling at the users' request; some users are content with the scene-center solar elevation angle in the metadata, while others prefer to calculate their own per-pixel solar elevation angle across the entire scene. Once a solar elevation angle is chosen, the conversion to true TOA reflectance is as given in equation (3).

$$\rho_\lambda = \frac{\rho'_\lambda}{\cos\theta_{sz}} = \frac{\rho'_\lambda}{\sin\theta_{se}} \quad (3)$$

Where

ρ_λ = Planetary TOA reflectance [unitless]

θ_{sz} = Local sun elevation angle; the scene centre sun elevation angle in degrees is provided in the metadata.

θ_{se} = Local solar zenith angle; θ_{sz} = 90°-θ_{se}

2.2.4. Cloud masking

Cloud masking was done by using Landsat Collection 1 Level-1 quality assessment band (QA). The Landsat Collection 1 Level-1 Quality Assessment (QA) 16-bit band allows users to apply per pixel filters to all Landsat Collection 1 Level-1 data products. Each pixel in the QA band contains unsigned integers representing bit-packed combinations of surface, atmospheric, and sensor conditions that can affect the overall usefulness of a given pixel. Landsat Collection 1 Level-1 QA bands (.TIF) are included in the Landsat Level-1 GeoTIFF Data Product downloaded from Earth Explorer (USGS, 2017). The QA band provides useful information on the cloud, cloud confidence, and cloud shadow confidence. The confidence levels of cloud and cloud shadow are divided into three levels: low, medium, and high, equivalent to 0%-33%, 34%-46%, and 67%-100%, respectively (USGS, 2017).

2.3. Methods

We consider that natural forest mapping is a contiguous forest, which was undisturbed during its existence. This classification concept requires classifying the study area into at least two classes: natural forest and non-natural forest areas. The procedure, therefore, is broken down into two major steps: classification of land cover and accumulation of bare land areas across time. We assume that natural forest changes are caused by human activities in timber logging or conversion to agricultural or developed land. Selective timber logging converts closed to open forest while clear-cutting or converting forestland to other land-use forms always experiencing a period when forestland changed to bare land. Hence, the detection of bare land is one of the steps for the classification of non-natural forest areas.

2.3.1. Simplified Spectral Patterns

The simplified spectral pattern (SSP) concept has been used for automated classification of land cover and water body extraction with Landsat images (Duong, 2018, 2016; Duong et al., 2017). An SSP is a transformation of the full spectral pattern into a simplified digital form, allowing direct incorporation of the spectral pattern into the classification. The SSP is constructed by a non-repetitive pairwise comparison of reflectance values between two bands (Charalambides, 2002). Given a pixel value vector B6={b1,b2,b3,b4,b5,b6}, where b1, b2,...,b6 denote top of atmosphere (TOA) reflectance of bands 2, 3, 4, 5, 6, and 7 of OLI, and bands 1, 2, 3, 4, 5, and 7 of ETM+ sensor, respectively. The simplified spectral pattern is defined by a new 15-digit vector, shown in equation (4).

$$m_{1,2}m_{1,3}m_{1,4}m_{1,5}m_{1,6}m_{2,3}m_{2,4}m_{2,5}m_{2,6}m_{3,4}m_{3,5}m_{3,6}m_{4,5}m_{4,6}m_{5,6} \quad (4)$$

where $m_{i,j}$ is the result of comparison between the reflectance of b_i and b_j and has values of 0 (if $b_j<b_i$.), 1 (if $b_j=b_i$), or 2 ($b_j>b_i$).

An example of SSP construction is presented in Fig. 2.

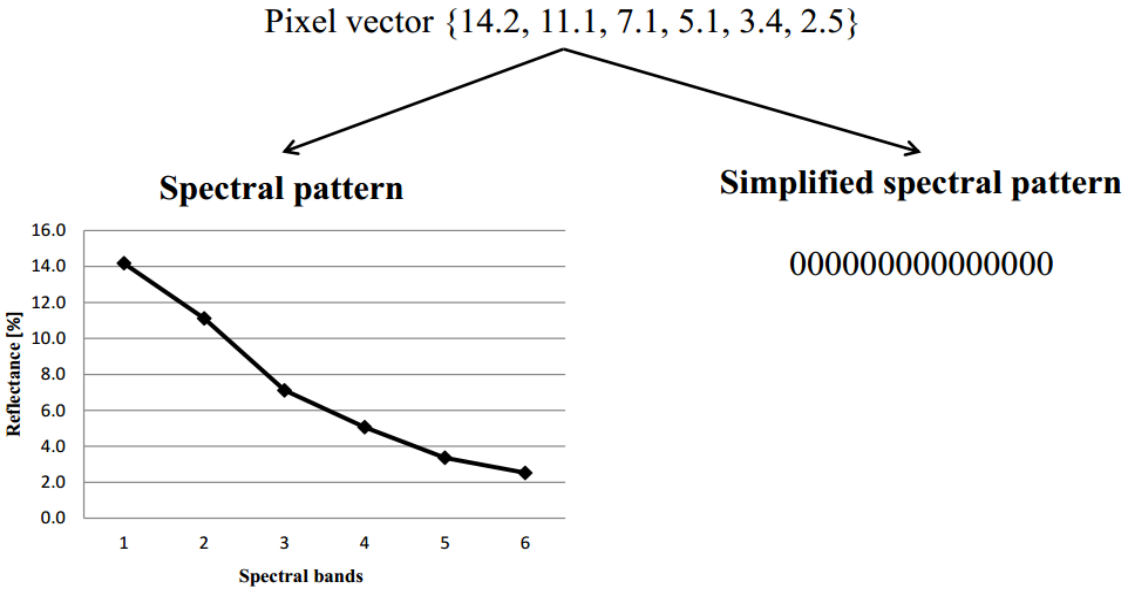

Figure 2. Example of a transformation of the spectral pattern into a simplified spectral pattern

2.3.2. Development of Simplified Spectral Pattern Database of Major Land Cover Classes

To facilitate the automation of land cover classification, we need to develop a database of major land cover classes. Due to slight differences in spectral characteristics of sensors TM, ETM+, and OLI, we have to develop different databases of SSP for major land cover categories for each sensor. These databases are used for the classification of single-date Landsat images. The following categories are included in the databases: cloud, cloud shadow, water, wetland, mangrove, and green vegetation, and brown vegetation, deciduous woodland, and dry, bare land. Due to the complexity of land cover characteristics, each land cover class involves one or more SSPs. Identification of SSP for each land cover class was realized by visual interpretation. A special software tool was developed for this purpose. The database of SSPs for the TM sensor contains 45 SSPs. For ETM+, there are 46 SSPs in the database, and for OLI, the database has 43 SSPs in total. Table 1 shows examples of SSPs for three land cover classes dark green vegetation, bright green vegetation, and dry, bare land for all three Landsat sensors.

In our method, every land cover class is recognized primarily by an SSP. However, to identify more specifically a particular class of land cover, we need to use some supporting variables computed using TOA reflectance. There are seven variables, which help us to describe better a shape of a spectral pattern. A list of those variables is given in Table 2.

Table 1. Examples of SSPs for three land cover classes DGV-dark green vegetation, BGV-bright green vegetation and DBL-dry bare land

Land cover class	Simplified Spectral Pattern		
	TM sensor	ETM+ sensor	OLI sensor
DGV	002200220220000 002000220220000	002200220220000	002200220222000
BGV	002200220220000 002200220222000 002200222222000 202200220222000 202220222222000	002200220220000 002200220222000 002200222222000 202200220222000 222200220220000 202200220220000	002200220222000 002200222222000 022222222222000 202220222222000 202200220222000 202200220220000
DBL	002222222222200 002220222222200 022222222222200 222222222222200 022222222222000 002200222222200 222222222222000 000220222222222 002222222222220 222222222222220 222222222220200	002220222222200 002222222222200 022222222222200 222222222222200 022222222222000 002202222222000 222222222222000 022222222222220 002222222222220 222220222222200 222222222222220 222220222222000 222222222220200 002200222222200	022222222222200 022222222222200 002222222222200 002222222222200 022222222222220 222222222222220 222222222222200 002222222222220 002200222222200 222222222220200 002220222222220

Table 2. List of variables that support a better description of a shape of a spectral pattern. B1---B6 denote TOA reflectance for bands blue, green, red, near infrared, short infrared 1and shortwave infrared 2 respectively

Variables	Formula
T_1	$(B_1+2*B_2+B_3)/2$
T_2	$(B_4+2*B_5+B_6)/2$
R_1	B_5/B_4
R_2	$2*B_5/(B_4+B_6)$
R_3	B_5/B_3
R_4	B_5/B_2
R_5	B_4/B_5

The number of supporting variables needed to identify a land cover class is not fixed for all classes. Some classes, such as clear water, do not need any supporting variables. Some other classes with a high probability of mixture with other classes such as wetland or dry, bare land require supporting variables. The database of SSPs, therefore, contains both SSPs and supporting variables for every land cover class. An example of using a software tool to identify SSP and supporting variables for a pixel in an image is given in Fig. 3.

2.3.3. Automated Classification of Land Cover and Natural Forests

The algorithm for the automated classification of land cover is straightforward. Figure 5 shows major steps for the classification of land cover using the database of SSPs. The algorithm is a simple loop of two computation steps: conversion of pixel value vectors to TOA reflectance and comparison of SSPs and supporting variables of a pixel with SSPs and supporting variables pre-determined in the database. Computation of TOA reflectance is conducted differently

for Landsat sensors using the information provided in the metadata files. The complexity of spectral characteristics of surface materials results in pixels with SSPs not yet defined in the databases. These pixels are classified to an unknown class as usual in the practice of image classification. If the number of unknown pixels is too large and those pixels threaten the quality of the classification result, we need to identify a new SSP and update the database of SSP to reduce unknown pixels in the classification result. If there is still a small number of unknown pixels after classification, spectral matching could be applied to fill those unknown pixels.

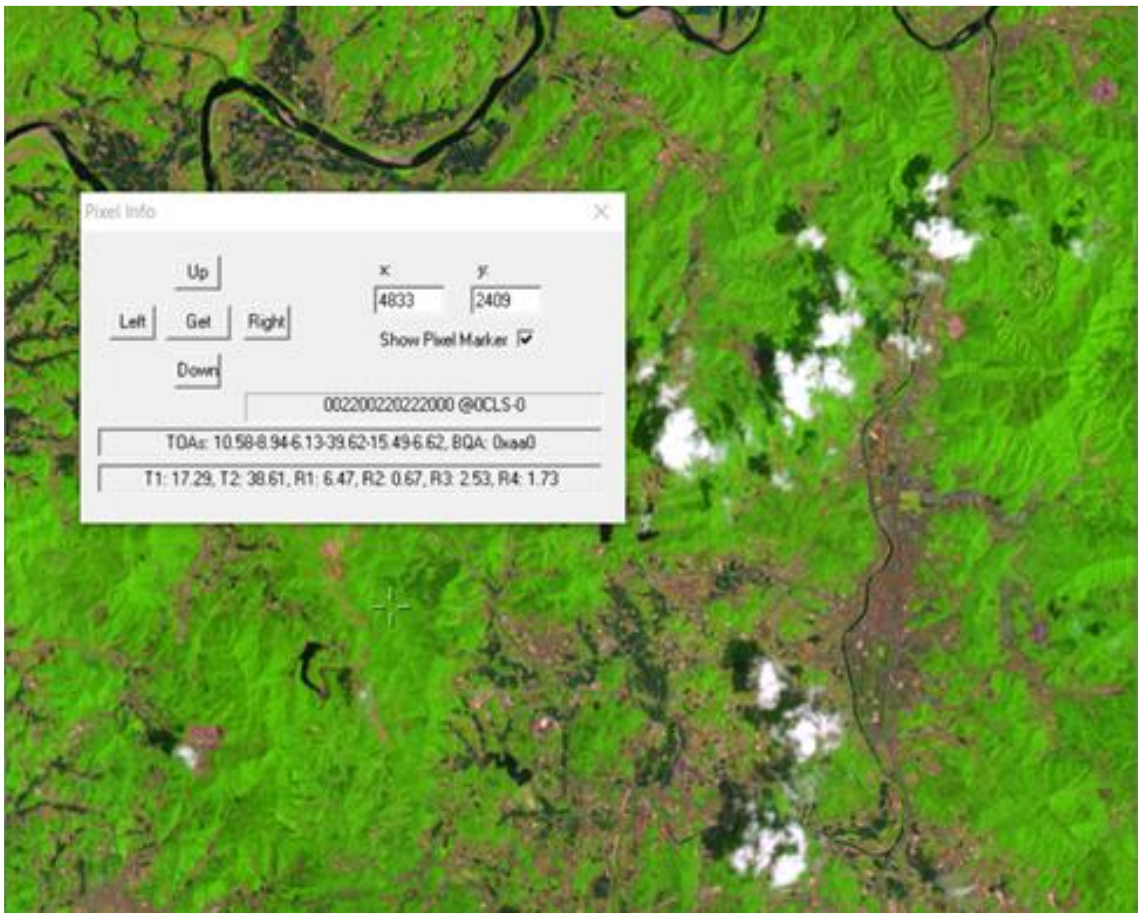

Figure 3. Example of using a software tool to identify SSP and supporting variables. The Pixel info window shows SSP code, number of SSP codes available within the image, pixel vector in TOA reflectance, and values of seven supporting variables

2.3.4. Stacks of Images within one year

Landsat images of tropical regions are always disturbed by clouds. It is inevitable facts. Clouds and cloud shadows must be reliably identified if we need to achieve a good result of the classification of land cover with Landsat time series. To reach a cloud-free land cover map in a certain period (dry or wet season), we need to classify more Landsat

images and stack them together. Information on clouds and cloud shadows can be extracted from band quality assessment (BQA) associated with every Landsat image in Landsat collection 1 (USGS, 2019b, 2017). Using the BQA, we can identify cloud and cloud shadow pixels in one image and replace them with clear pixels from images of another date in the Landsat time series. Figure 4 demonstrates the stacking of classified images to create cloud-free classified images.

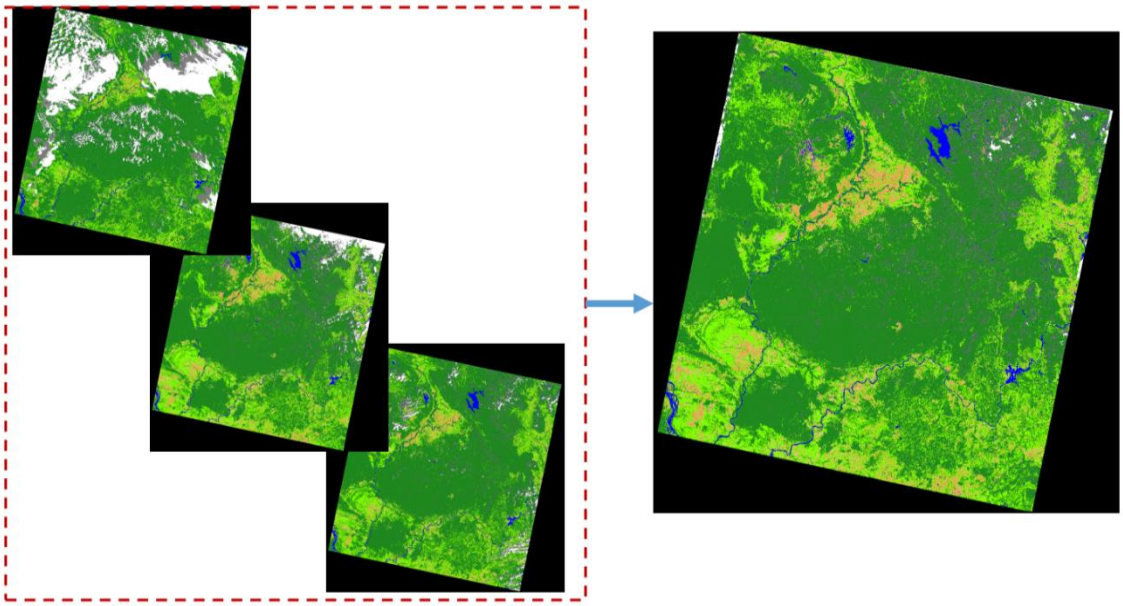

Figure 4. Demonstration of image stacking to create a cloud-free classified image. Single date classified images are in the left side block. After stacking, a cloud-free image is created and shown in the right side block

2.3.5. Natural Forests Extraction

We assume that a natural forest is a forest that is not substantially changed during its existence except the consequence of hazards like landslides or fire. This assumption redirects natural forest detection to detection of forest change to bare land during its existence. In the study area, two prevalent forest covers evergreen and dry deciduous forest. Dry deciduous forest has a leaf-off season from late December to April of the next year. During that period, the dry deciduous forest looks like bare land on the Landsat image. To avoid miss classification, we do not collect Landsat images of the area with distribution of dry deciduous forest. We accumulate classified images of one year to find changed and unchanged forest covers. When we stack multiple-year classified images, again, we can mark changed and unchanged forest covers. The long-time unchanged forest cover is then classified as natural forest cover Fig. 5. Displays flow chart of an algorithm for automated classification of land cover and natural forest mapping

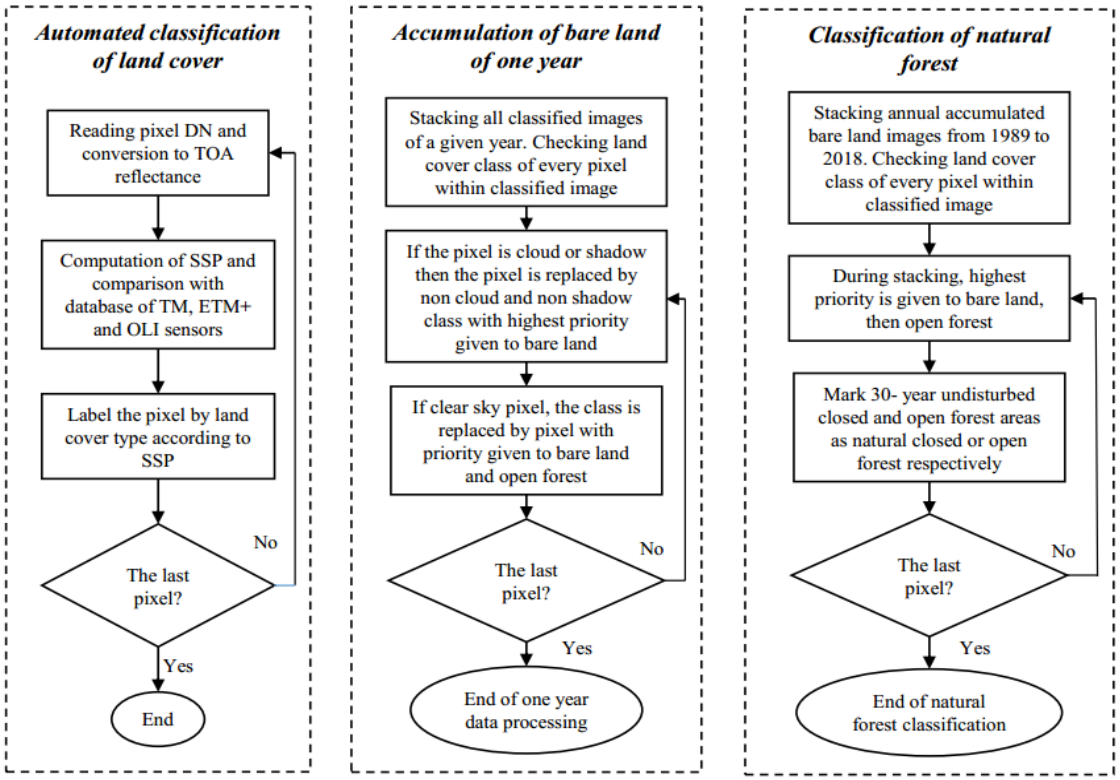

Figure 5. Flow chart of an algorithm for automated classification of land cover and natural forest mapping

3. Result and Discussion

The method for natural forest mapping was implemented using C++ language for applications in Windows 32-bit and 64-bit environments. The software running in command mode allows batch processing of a large amount of Landsat images. All Landsat Collection 1 level-1 images of the study area from 1989 to 2018 were selected for classification. About 2000 images were analyzed, stacked and subset, and mosaicked according to the boundaries of provinces. We created an annual land cover map for each province with four classes: closed natural forest CNF, open natural forest ONF, water, and area of intense human activities IHA. The class IHA includes forest plantation, industrial trees, crop and paddy fields, and human settlements. A set of 30 annual land cover maps provides Spatio-temporal changes of the three classes CNF, ONF, and IHA from 1989 to 2018 in the study area. Quantitative analysis of changes of natural forest reveals trends of land use in Cambodia, Laos, and Vietnam in the past 30 years.

3.1. Ratanakiri province

In Ratanakiri, the natural closed forest was reduced from 958,575 ha in 1989 to 466,529 ha in 2018, equivalent to a loss of 51.3% (annual 1.7%). The closed natural forest was replaced by open natural forest and areas of intense human activities. The open natural forest was increased from 277,796 ha in 1989 to 530,814 ha in 2018, equivalent to a gain of 91.1%, while the area of intense human activities increased from 31,495 ha in 1989 to 273,830 ha in 2018, equivalent to a gain of 769.4%. Figure 6 shows changes in the natural forest of Ratanakiri from 1989 to 2018.

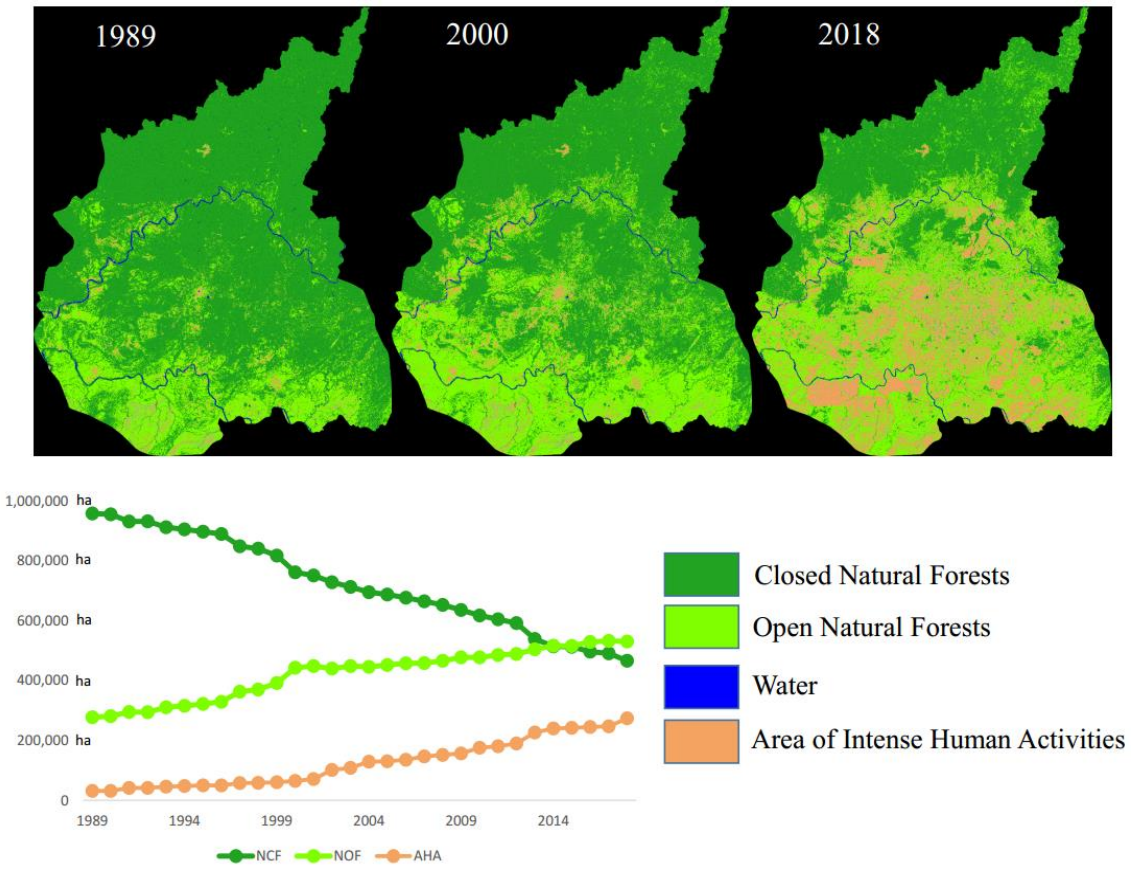

Figure 6. 30-year change of natural forests in Ratanakiri province of Cambodia. Three classified images in the upper part of the figure show land cover data in 1989, 2000, and 2018. The graph in the lower part visualizes quantitative changes in closed and open natural forests and areas of intense human activities

Graphs in Fig. 6 show interesting patterns of closed and open natural forests and areas of intense human activities. Closed natural forests continuously decrease while open natural forests and areas of intense human activities increase incessantly.

3.2. Attapeu province

Natural closed forest in Attapeu was decreased from 879,005 ha in 1989 to 634,557 ha in 2018, equivalent to loss of 27.8% (annual 0.93%). The natural open forest was extended from 90,752 ha in 1989 to 231,830 ha in 2018, equivalent to 155.4%. The area under intensive human activities increased from 23,957 ha in 1989 to 138,675 ha in 2018, equivalent to a gain of 478.8%. Figure 7 presents analysis results of land cover changes for Attapeu province.

3.3. Kon Tum province

Natural closed forest in Kon Tum was reduced from 848,307 ha in 1989 to 424,388 ha in 2018, equivalent to a loss of 50% (annual 1.7%). The natural open forest was enlarged from 78,629 ha in 1989 to 224,963 ha in 2018, equivalent to a gain of 186.1%. The area under intensive human activities increased from 40,098 ha in 1989 to 320,354 ha in 2018, equivalently to a gain of 698.9%. Figure 8 displays 30-year changes of natural closed and open forests of Kon Tum province.

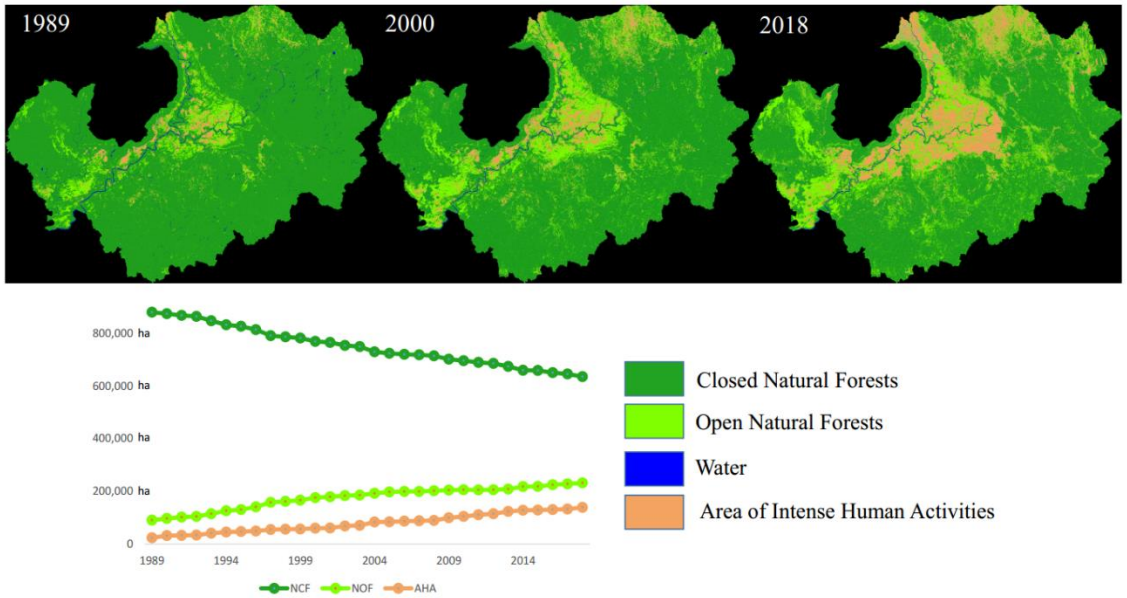

Figure 7. 30-year change of natural forests of Attapeu province of Laos. Three classified images in the upper part of the figure show land cover data in 1989, 2000, and 2018. The graph in the lower part visualizes quantitative changes in closed and open natural forests and areas of intense human activities

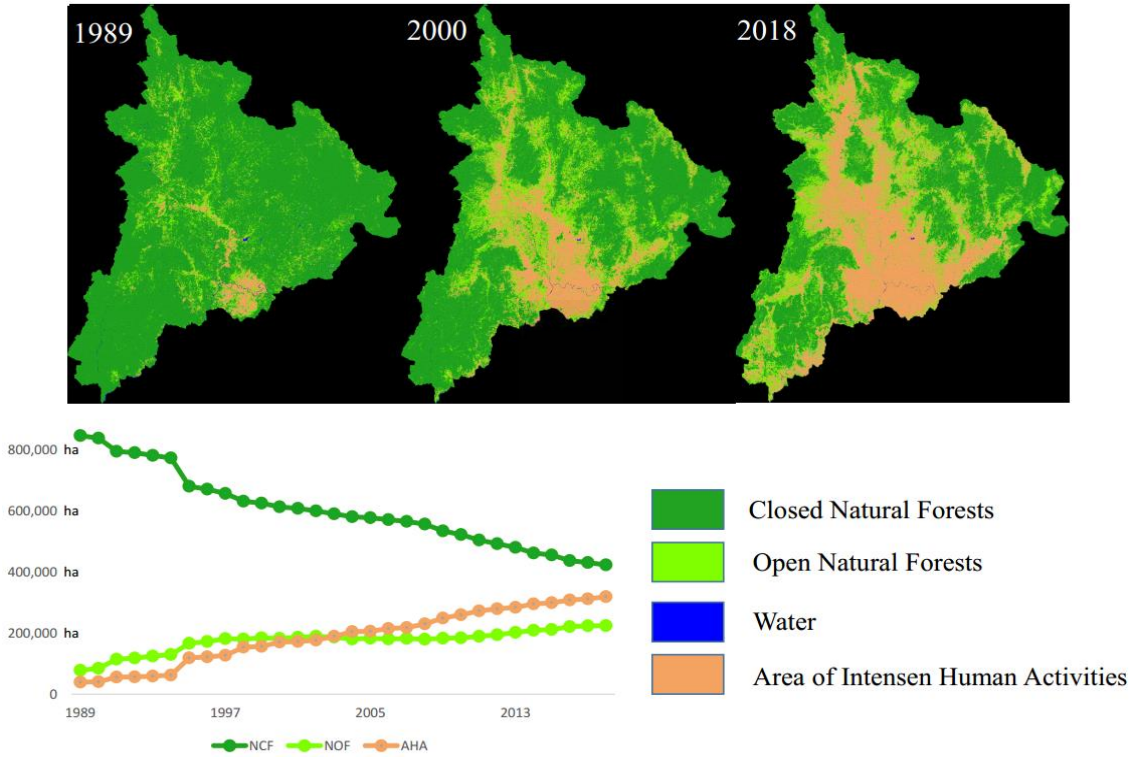

Figure 8. 30-year change of natural forests of Kon Tum province of Vietnam. Three classified images in the upper part of the figure show land cover data of 1989, 2000, and 2018. The graph in the lower part visualizes quantitative changes in closed and open natural forests and areas of intense human activities

3.4. Validation

The validation of classification results for natural forests was possible only for the year 2018. It is hard to validate the reliability of classification for past years. We conducted a field survey in December 2018 and March 2020 to collect ground data for classification accuracy analysis. Because in our proposed method, the spectral pattern was used as the major classification criteria, so the validation of classification results is equal to the validation of spectral patterns and their simplified forms. Field survey in 2018 and the use of the high spatial resolution imagery of Google Earth showed very high accuracy of 2018 land cover maps. Using Create random point function of ArcGIS, we created 50 points for each province for validation and imported these points to Google Earth for visual interpretation. Figure 9 shows the spatial distribution of points in each province in ArcGIS and Google Earth. Agreement of classification results and visual interpretation is very high. Among 150 points, natural forests were correctly classified in 149 points, and only one point was miss classified. This results in total accuracy are 99.3%.

We assume that spectral patterns of ground materials observed by Landsat sensors are stable across time. Hence, we expect that classification results of Landsat images in past years have high reliability.

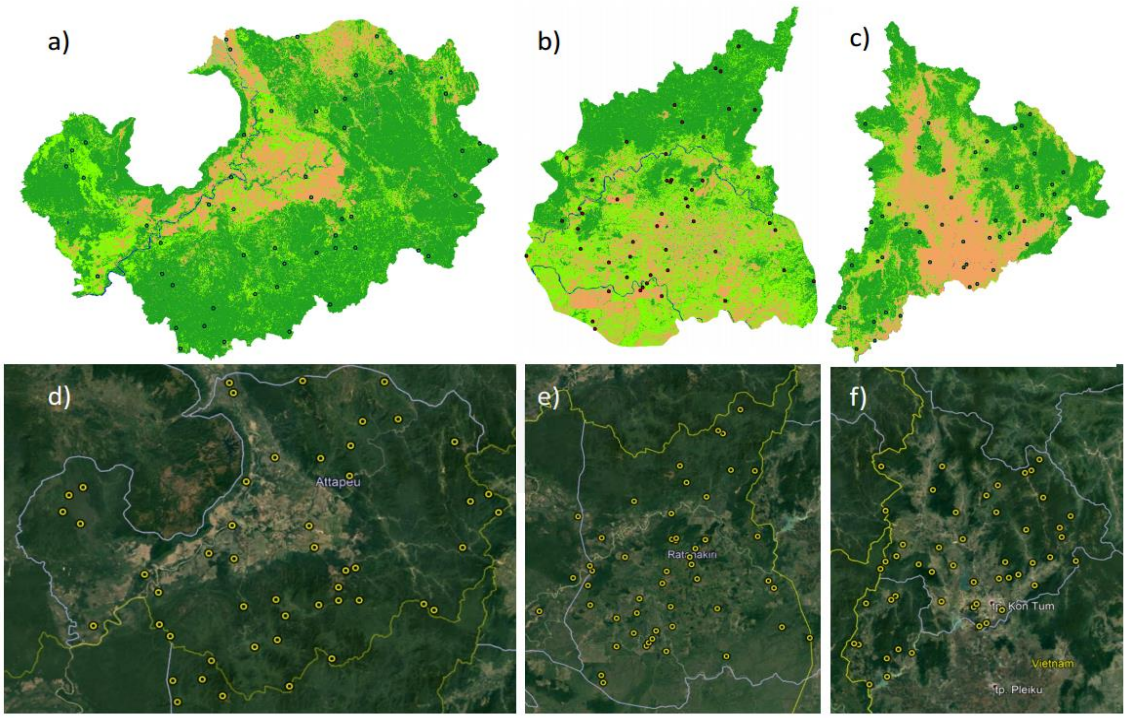

Figure 9. Spatial distribution of points for validation of classification results of the year 2018. a), b), and c) are classification results of the year 2018 with validation points in black color for Attapeu, Ratanakiri, and Kon Tum. d), e) and f) illustrate validation points imported to Google Earth to validate classification accuracy by visual interpretation using high-resolution imageries. The number of validation points for each province is 50 created by Create random points function in ArcGIS

3.5. Discussions

The transition process of natural forests takes place in three types. Type 1: direct transition of closed natural forests to other land use, type 2: transition of closed natural forests to a degraded forest, and type 3: transition of open natural forests to other land use. The direct transition of natural forests to another land like forest plantation, cultivation, or infrastructure development exhibits intensive exploitation of forest land. In contrast, the transition of natural forests to degraded (open) forests shows prevalently illegal logging (selective cutting). Depending on each country's land management system and development level, the transition of forest forms may have different characteristics. Cambodia, Laos, and Vietnam are countries of different land management systems, so processes of forestland transition to another land in each country are contrasting.

In Ratanakiri, graphs of closed natural forests and open natural forests run in opposite directions and intersect in 2015. This pattern discloses the intensive transition of closed natural forests to open natural forests. In 1989, closed natural forests were 3.5 times larger than closed natural forests, but in 2018, the area of closed natural forests was 0.98 times smaller than that of open natural forests. On the other hand, the graph of open natural forest runs parallel with the graph of the area of intense human activities but shifts in a higher position above the graph of the area of intense human activities. The large discrepancy in area values between open natural forests and areas of intense human activities reveals that the transition of open natural forests to intense human activities takes place quite slowly. The total effect of the rapid decrease of closed natural forests, the rapid increase of open natural forests, and the slow rise of the area of intense human activities conclude degradation of closed natural forests by selective cutting is a major tendency in Ratanakiri.

In Attapeu, the graph of closed natural forests is located in a much higher position than open natural forests, showing an overwhelming majority of closed natural forests versus open natural forests. The trend of the closed natural forest graph is slightly declining while the tendency of the open natural forests graph is in the opposite direction. Interesting is that the graph of the area of intense human activities is located in a position very near the graph of open natural forests, just slightly below. These graphs slowly rise in parallel across time. This pattern of the graphs demonstrates slight deforestation in Attapeu and conversion of natural forests to another land. The transition types are mostly of types 2 and 3.

In Kon Tum, all three graphs manifest intensive land exploitation in this area. Graph of the closed natural forests descends fast while the open natural forests graph raises at almost the same rate. However, interesting is that the area of intense human activities raises much faster than open natural forests, and both graphs intersected in the year 2003. This pattern of graphs reveals all three forest transition types are presented in Kon Tum. However, there is a strong direct conversion of closed natural forests to another land.

4. Conclusions

In this paper, we applied a new algorithm for automated land cover classification with Landsat time series to assess 30-year changes of natural forest cover in Cambodia, Laos, and Vietnam. We selected three provinces from Cambodia, Laos, and Vietnam for case studies. All Landsat scenes with path/ row numbers 124/49, 124/50, 124/51, 125/50, and 125/51 from 1989 to 2018 have been used for classification. The total number of images was about 2000 scenes. In this research, we considered forest cover, which was not long

time disturbed as natural forests. We monitored changes of three principal classes: closed natural forest, open natural forest, and area of intense human activities in every province in the study area for years from 1989 to 2018 and constructed graphs presenting changes. We randomly generated 150 points to validate classification for the year 2018 using visual interpretation with high spatial resolution imagery of Google Earth. Overall accuracy was 99.3%. After 30 years, natural forests decrease in all three provinces at different rates. Natural forests lost 51.3% in Ratanakiri, 27.8% in Attapeu, and 50% in Kon Tum. Patterns of graphs for each province reveal much information about forest transition drivers. Prevalent forest change in Ratanakiri was a change of closed natural forest to open natural forest. It looks like selective cutting was the main driving force. In Attapeu, there was slight deforestation, and conversion of open natural forest to other land use was a major trend. In Kon Tum, all types of forest transitions were presented. The closed natural forest changed to open natural forest, other lands, and open natural forest changed to another land. However, there was a sign of strong direct conversion of closed natural forests to another land.

The methodology presented in this paper formulates a foundation for the development of a uniform method for forest cover monitoring in a large area using the Landsat time series.

Acknowledgments

A grant number TN18/T09 under the research program KHCN-TN/16-20 from the Vietnam Academy of Science and Technology has supported this research.

References

Banskota A., Kayastha N., Falkowski M.J., Wulder M.A., Froese R.E., White J.C., Banskota A., Kayastha N., Falkowski M.J., Michael A., Froese R.E., White J.C., Monitoring F., Landsat U., Banskota A., Kayastha N., Falkowski M.J., Michael A., Froese R.E., White J.C., Forest C., Pacific S., Centre F., Canada N.R., 2014. Forest Monitoring Using Landsat Time Series Data : A Review Forest Monitoring Using Landsat Time Series Data : A Review, 8992, 362-384. https://doi.org/10.1080/07038992.2014.987376.

Charalambides C.A., 2002. Enumerative Combinatorics, in: Enumerative Combinatorics, 40-42.

Coppin P.R., Bauer M.E., 1996. Digital change detection in forest ecosystems with remote sensing imagery Digital Change Detection in Forest Ecosystems with Remote Sensing Imagery. Remote sensing reviews, 13, 207-2341. https://doi.org/10.1080/02757259609532305.

Dennis R.A., Meijaard E., Nasi R., Gustafsson L., 2008. Biodiversity Conservation in Southeast Asian Timber Concessions : a Critical Evaluation of Policy Mechanisms and Guidelines. Ecology and Society, 13.

Duong N.D., 2016. Automated classification of Land cover using Landsat 8 OLI Surface Reflectance product and spectral pattern analysis concept - Case study in Hanoi, Vietnam. International Archives of the Photogrammetry, Remote Sensing and Spatial Information Sciences - ISPRS Archives, 41, 987991. https://doi.org/10.5194/isprsarchives-XLI-B8-987-2016.

Duong N.D., 2018. Decomposition of Landsat 8 OLI Images by Simplified Spectral Patterns for Land Cover Mapping. 2018 10th IAPR Workshop on Pattern Recognition in Remote Sensing (PRRS), 1-13.

Duong N.D., 2020. Automated classification of natural forests with Landsat time series uisng simplified spectral patterns, in: Int. Arch. Photogramm. Remote Sens. Spatial Inf. Sci, XLIII-B3-2020, 983-988. https://doi.org/https://doi.org/10.5194/isprs-archives-XLIII-B3-2020-983-2020.

Duong N.D., Hang L.M., Tuan T.A., Ouyang Z., 2017. Development of a spectral-pattern-analysis-based method for automated water body extraction using Landsat image data: A case study in central Vietnam and southern Laos. Limnology and

Oceanography: Methods, 15, 945-959. https://doi.org/10.1002/lom3.10215.

FAO, 1995. FAO: Forest Resources Assessment 1990: Global Synthesis: FAO Forestry Paper 124.

FAO, 2005. State of the World's Forests.

Hughes A.C., 2017. Understanding the drivers of S outheast A sian biodiversity loss. Ecosphere 8, e01624. 10.1002/ecs2.1624.

Stibig H., Stolle F., Dennis R., Feldkötter C., 2007. Forest Cover Change in Southeast Asia - The Regional Pattern -. Biogeosciences.

USGS, 2015. Landsat 8 (L8) Data Users Handbook. Earth Resources Observation and Science (EROS) Center.

USGS, 2017. USER GUIDE LANDSAT QUALITY ASSESSMENT (QA) TOOLS.

USGS, 2019a. Landsat 8 (L8) Data Users Handbook. Book 8.

USGS, 2019b. LANDSAT COLLECTION 1 LEVEL 1 PRODUCT DEFINITION Version 2.0.

White C.J., Wulder M.A., Hobart G.W., Luther J.E., Hermosilla T., Griffiths P., Guindon L., 2014. Pixel-Based Image Compositing for Large-Area Dense Time Series Applications and Science Pixel-Based Image Compositing for Large-Area Dense. Canadian Journal of Remote Sensing, 40, 192-212. https://doi.org/10.1080/07038992.2014.945827.